# Characterization and hydrodesulfurization activity of CoMo catalysts supported on sol-gel prepared Al2O3

Franck Dumeignil, Koichi Sato, Motoyasu Imamura, Nobuyuki Matsubayashi, Edmond Payen, Hiromichi Shimada

# Characterization and hydrodesulfurization activity of CoMo catalysts supported on sol-gel prepared $Al_2O_3$

Franck Dumeignil[a]*, Koichi Sato[a], Motoyasu Imamura[a], Nobuyuki Matsubayashi[a], Edmond Payen[b], Hiromichi Shimada [a]**

[a] National Institute of Advanced Industrial Science and Technology (AIST)

Higashi 1-1-1, Tsukuba, Ibaraki 305-8565 (Japan)

[b] Laboratoire de Catalyse de Lille UMR CNRS 8010

Université des Sciences et Technologies de Lille (USTL), Bâtiment C3

59655 Villeneuve d'Ascq Cedex (France)

*: Present address: Department of Chemical Engineering, Tokyo University of Agriculture and Technology, 2-24-16 Nakacho, Koganei, Tokyo 184-8588, Japan

**: Corresponding author, Tel: +81-298-61-6258, FAX: +81-298-61-2371

Email: h-shimada@aist.go.jp

**Abstract**

A series of $CoMo/Al_2O_3$ catalysts was prepared by impregnation on a series of alumina powders synthesized by the sol-gel method with different hydrolysis ratios R (defined as [$H_2O$] / [aluminum-tri-sec-butoxide (ASB)]; R = 3, 4, ..., 12, 13). The oxide precursors were characterized and subsequently tested in the hydrodesulfurization (HDS) of thiophene, dibenzothiophene (DBT), and 4,6-dimethyldibenzothiophene (4,6-DMDBT). Mainly due to their large pore diameters of *ca.* 6 nm, the catalysts prepared from the alumina with hydrolysis ratio R = 7 ~ 10 showed higher HDS activity compared with the activities of the other prepared catalysts. The effect of the pore diffusional limitation was more significant than expected, due to the ink-bottle shape of the pores of the prepared catalysts with hydrolysis ratio R < 8 and R > 10. Due to highly dispersed CoMo active phase, the HDS activity of the prepared catalysts with hydrolysis ratio R = 8 and 9 for thiophene was similar to that of a reference industrial catalyst that was designed and manufactured for deep HDS of diesel fuel fractions. Furthermore, the HDS activity of the prepared catalysts with hydrolysis ratio R > 5 for DBT was higher than that of the reference industrial catalyst. For 4,6-DMDBT, however, the reference industrial catalyst showed higher HDS activity compared with the activities of the prepared catalysts. Relatively high HDS activity was observed for the prepared catalysts with R = 9 and 10 with cylindrical pore shape and with a high proportion of strong acid sites. The strong acidity supposedly enhanced the hydrogenation activity of the catalysts that was essential for the HDS of 4,6-DMDBT.

**Keywords**

Catalysis, sol-gel, alumina, CoMo, HDS, porosity, acidity, thiophene, DBT, 4,6-DMDBT

## 1. Introduction

The increasing demand for protection of the environment has been the impetus behind the improvement in performance of hydrodesulfurization (HDS) catalysts to produce clean fuels. In fact, legal limitations on the sulfur content in fuels are becoming more stringent and require oil refineries to reduce the sulfur content in their commercial products. For example, sulfur content in diesel fuel in European countries has been reduced from 350 ppm to 50 ppm in 2005 [1]. To meet this new regulation, the most refractory sulfur species that have been identified as 4,6-dimethyldibenzothiophene (4,6-DMDBT) -type compounds must be desulfurized [2-5], because these compounds represent the major part of sulfur remaining in the feed after treatment by conventional HDS processes.

To achieve HDS of 4,6-DMDBT, several new strategies have been investigated, most of which have focused on the development of new catalysts. Although Co-Mo-S or Ni-Mo-S catalysts supported on $\gamma$-$Al_2O_3$ have been the most widely used in HDS of oil fractions, significant effort to improve the active phase by, for example, incorporation of noble metals, has been reported [6-22]. Several new supports, such as $TiO_2$ or mixed oxides [23-42], carbon [43], and zeolites [44], in combination with Co-Mo-S or Ni-Mo-S as the catalytically active phase have also been investigated. In contrast, improvement in $\gamma$-$Al_2O_3$ supports by applying new preparation methods has not been extensively researched presumably due to a greater interest in preparing new active phases or / and new supports. Among new preparation methods for $\gamma$-$Al_2O_3$, the sol-gel synthesis method is of particular interest, because this method enables the preparation of $\gamma$-$Al_2O_3$ with both high surface area (SA) and large pore diameters (PD), provided that the

preparation parameters, such as temperature and ratio of reactants, are correctly chosen. For example, Dumeignil and Grimblot recently reported that Co-Mo catalysts supported on a sol-gel prepared $\gamma$-$Al_2O_3$ support showed a remarkable increase (about 60 %) in the catalytic activity for HDS of thiophene compared with an industrial CoMo catalyst with the same formulation [45]. In a subsequent work [46], Dumeignil *et al.* studied the effect of the hydrolysis ratio R (defined as [$H_2O$] / [aluminum-tri-sec-butoxide (ASB)]) during the sol-gel synthesis on the properties of the prepared $\gamma$-$Al_2O_3$ powders to optimize the preparation parameters of the catalyst support for HDS applications. Their study showed that for $3 \leq R \leq 13$ (3 being the stoichiometric ratio), the average PD of the $\gamma$-$Al_2O_3$ powders was larger than 3 nm and the water pore volume (PV) was larger than 0.9 $cm^3.g^{-1}$, both of which are desirable in catalyst supports. The powders obtained for $R \approx 9$ possessed the largest average PD (about 9 nm) with pseudo-cylindrical features, whereas the pores for other R values showed ink-bottle-type features. In addition, the powders for $R \approx 9$ exhibited stronger acidity compared with the other powders.

The aim of the present study was to clarify the effect of R on the catalytic activity of CoMo HDS catalysts supported on these sol-gel prepared alumina powders prepared by Dumeignil *et al.* [46]. For this purpose, CoMo HDS catalysts were prepared by incipient wetness impregnation of the aforementioned series of sol-gel prepared $\gamma$-$Al_2O_3$ supports [46]. First, oxidic precursors and sulfided catalysts were characterized by physico-chemical techniques; porosimetry was used to characterize the textural properties, and Raman spectroscopy and high-resolution electron microscopy (HREM) were used to elucidate the nature of the oxidic and sulfided active phases. Then, catalytic activity tests were performed using thiophene, dibenzothiophene (DBT), and 4,6-DMDBT as the

probe molecules. Finally, the catalytic activities were evaluated in relation to the physico-chemical properties of the prepared catalysts.

## 2. Experimental

### 2.1. Catalyst preparation

The $Al_2O_3$ supports were synthesized using a sol-gel method from aluminum-tri-sec-butoxide (ASB) complexed with butane-1,3-diol with a [ASB] / [butane-1,3-diol] ratio of 2. The hydrolysis step was done by mixing water and ASB with various values of R (defined as $[H_2O]$ / [ASB]), R = 3, 4, 5…, 12, and 13. The detailed preparation procedures were described elsewhere [46]. Table 1 shows the textural and acidic properties of the $Al_2O_3$ supports.

The $CoMo/Al_2O_3$ oxidic precursors were prepared by one-step incipient wetness impregnation of these $Al_2O_3$ supports with an aqueous solution of $(NH_4)_6Mo_7O_{24},6H_2O$ and $Co(NO_3)_3,6H_2O$. The Mo loading was chosen at 10 wt% as metallic Mo with a fixed Co / (Co + Mo) ratio (α) of 0.4 (equivalent to 4.1 wt% Co as metallic Co), because this formulation has yielded the highest catalytic activity in the HDS of thiophene using a sol-gel $Al_2O_3$ support prepared with R = 10 [45]. The catalytic activities were compared with those for a commercially available $CoMo/Al_2O_3$ industrial catalyst with 15 wt% Mo loading whose detailed characteristics were confidential. Before the catalytic activity tests, the catalyst powders were compressed and sieved to yield powders from 0.2 mm to 0.35 mm to minimize the effects of the particle size on the catalytic activity.

### 2.2. Catalyst characterization

*Porosimetry*

$N_2$ adsorption and desorption isotherms of the oxidic precursors (*i.e.* catalysts in the oxide state, before presulfidation) were measured using a Micromeretics ASAP 2010 system. BET surface area (SA) and BJH pore volume (PV) were calculated using the software provided with this system.

*Laser Raman spectroscopy*

The Raman spectra of the oxidic precursors were recorded between 200 and 1400 $cm^{-1}$ on a LabRam Infinity spectrometer. The excitation power of the 532 nm line of the YAG laser was fixed at 5 mW.

*High Resolution Electron Microscopy (HREM) observation*

The catalyst powders were ultrasonically dispersed in hexane on a microscope grid covered with a thin carbon holed film. Then, HREM photographs of the sulfided catalysts were obtained using a Hitachi H-9000 with an instrumental resolution of about 0.5 nm. Statistical analysis of each HREM photograph was done by measuring the length (L) and number (N) of about 400 $MoS_2$ slabs according to the method by Payen *et al.* (*e.g.*, [47]).

2.3. Catalytic activity tests

*HDS of thiophene*

Catalytic activity for HDS of thiophene was measured at atmospheric pressure in a flow-type reactor packed with 0.2 g of catalyst. Before reaction, the oxidic precursors were sulfided at 673 K for 2 h under a flow (20 $cm^3.min^{-1}$) of $H_2S$ / $H_2$ (10 / 90) and then cooled to a reaction temperature of 573 K. After purification by two successive vacuum

distillations, thiophene was introduced into the reactor at a constant pressure of 6.65 kPa using a flow of hydrogen (20 $cm^3.min^{-1}$). The reaction products were analyzed using a gas chromatograph equipped with a flame ionization detector and a Plot-alumina column with a length of 50 m. The sensitivity for each compound was assumed at 3.4 for thiophene and at 4 for other C4 products. Therefore, the conversion, $\chi$, was calculated using the following formula:

$$\chi = \frac{\sum_{i=1}^{4} \frac{a_i}{4}}{\frac{a_t}{3{,}4} + \sum_{i=1}^{4} \frac{a_i}{4}} \qquad (1)$$

$a_i$ = *i product peak area*

$a_t$ = *thiophene peak area*

The catalytic activity per unit weight of catalyst was thus calculated using this equation and using $3.05 \times 10^{-7}$ $mol.g_{cat}^{-1}.s^{-1}$ as the initial molar flow rate of thiophene.

*HDS of DBT and 4,6-DMDBT*

Catalytic activity tests for HDS of DBT and 4,6-DMDBT were done at 603 K for 1 h using a batch reaction system. Before the reaction, the oxidic precursors were pre-sulfided at 673 K (reached at a rate of 360 $K.h^{-1}$) for 3 h under a flow of 10 % $H_2S$ in $H_2$ (20 $cm^3.min^{-1}$). DBT was diluted by n-tetradecane at 3 wt%, whereas 4,6-DMDBT was diluted with n-decane at 0.3 wt%. The reactor with an inner volume of 50 $cm^3$ was filled with 5 $cm^3$ of the reactant solution and hydrogen at 4 MPa (cold charge). Assuming first-order reaction kinetics, we estimated the reaction rate constant over each catalyst by

plotting *ln(1-conversion)* as a function of catalyst weight (0.01, 0.02, 0.05, and 0.1 g). Figure 1 shows a sample plot of the conversion versus catalyst weight. The catalytic activity per unit weight of catalyst was calculated using the slope of the line in Fig. 1 and the mole number of DBT or 4,6-DMDBT in the reactant solution. Based on the fluctuations of the plotted points, the error in the calculated activity was estimated at ± 5% for DBT and ± 7.5% for 4,6-DMDBT.

## 3. Results

### 3.1. Catalyst characterization

Table 2 shows the physical properties of the oxidic precursors. Both the SA and PV decreased after the loading of CoO and $MoO_3$ compared with those of the $Al_2O_3$ supports. The SA for R > 4 exceeded 340 $m^2.g^{-1}$ and was relatively constant at 345 ~ 395 $m^2.g^{-1}$. The relative decrease in SA by the loading of CoO and $MoO_3$ was between 5 % (for R = 11) and 25 % (for R = 12) except for R = 3, 9, 10, and 13. The SA for R = 3 significantly decreased (by more than 35 %), whereas that for R = 9, 10, and 13 slightly increased (by *ca.* 1 ~ 10 %). The PV increased with increasing R from 0.17 $cm^3.g^{-1}$ for R = 3 up to 0.63 $cm^3.g^{-1}$ for R = 10 and then slightly decreased to 0.50 ~ 0.60 $cm^3.g^{-1}$ for R > 10. This decrease in PV by the loading of Co and Mo was larger than the decrease in SA. In particular, PV was less than 50 % of the initial PV at R = 3.

Three mechanisms are responsible for these decreases in SA and PV. In the first mechanism, the loading of Co and Mo increased the weight of each particle. The calculated relative decrease in SA was 17 %, assuming that each particle gained weight by loading 15 % of $MoO_3$ and 5.2 % of CoO without any change in SA. In addition, the

deposition of $MoO_3$ and CoO inside the pores decreased PV. Assuming that all the $MoO_3$ and CoO with a density of 6.3 $g.cm^{-3}$ for crystallographic ideal compact structures were deposited inside the catalyst pores, the calculated relative decrease in PV was 21 % including the contribution from the particle weight-gain. In the second mechanism, sintering of $Al_2O_3$ supports might have occurred during calcination after CoMo loading. In the third mechanism, plugging at pore mouths by the deposition of $MoO_3$ and CoO might have significantly decreased both the SA and PV.

For R = 9 and 10, SA of the oxidic precursors was larger than that of the corresponding $Al_2O_3$ supports probably due to “bumpy structures” caused by the deposited $MoO_3$ and CoO; i.e, these bumpy structures caused by three-dimensionally developed CoMo oxidic particles added their own SA to that of the support itself. The SA of the precursors for other R, however, decreased by about 15 % after CoMo loading compared with their initial SA, probably due mostly to the first mechanism. The PV decreased by about 32 %, which is larger than that calculated assuming the first mechanism (17 %); this difference between the measured and calculated PV is likely due to overestimation of the theoretical density of $MoO_3$ and CoO, 6.3 $g.cm^{-3}$.

All the results presented in this section indicate that the decreases in SA and PV due to the second and third mechanisms were significant only for the prepared catalysts with hydrolysis ratio R = 3 and 4 with small average PD. In a previous report [46], we showed that ink-bottle-type pores are created among closely packed first-order particles in the sol-gel synthesis of $Al_2O_3$ for R < 9 and R > 10, and also showed that for R = 9 and 10, first-order particles are loosely packed and pseudo-cylindrical pores are formed in the interstitial spaces. Considering this, quantitative estimation of the relative participation of each mechanism in the decreases in SA and PV observed here indicates that the

number of ink-bottle type pores with small diameters decreased or that these ink-bottle pores totally disappeared by sintering or plugging by CoMo loading, whereas neither the ink-bottle-type nor cylindrical type pores with large diameters were significantly affected. Figure 2 shows that the average PD of the oxidic precursor increased with increasing R up to R=7 and then became relatively constant with further increase in R.

Figure 3 shows the Raman spectra of the oxidic precursors. The spectrum for R = 3 exhibited several sharp peaks, whereas the spectra for R > 4 exhibited a main broad peak between 700 and 1000 $cm^{1}$. According to the literature the sharp peaks observed in the spectra for R = 3 can be assigned to [a] $CoMoO_4$ phase [45, 48, 49], whereas the broad peak observed for R > 4 is characteristic of the monomolybdate phase (main line at 930 $cm^{-1}$) and / or the polymolybdate phase (main line at 952 $cm^{-1}$) [50-53]. The results of the Raman spectra therefore indicate that mono- or poly-molybdate species were well dispersed on the oxidic precursors except for R = 3.

Figure 4 shows the distribution of the lengths of $MoS_2$ slabs observed in the HREM images (not shown here) of the sulfided CoMo catalysts for R = 5, 10, and 11. No significant difference in this distribution was observed among the examined samples. Each distribution peak was centered at about 1.5 nm and had low percentages of slab lengths greater than 4 nm. Figure 5 shows the distribution of the number of stacked $MoS_2$ slabs observed in the HREM images of the same samples. For all the samples examined, single- and two-layered slabs were predominant, and slabs with four or more layers were minor. Most of the past studies [47, 54-56] report that, for conventionally prepared catalysts, the average number of stacked slabs did not exceed two layers and that the average slab length was about 3.0 nm.

The dispersion of $MoS_2$ particles on the catalysts prepared in our study, therefore,

was higher than, or at least not lower than those reported in the literature, although controversy still exists about the determination of slab length [57-59]. In addition, the effect of the $MoS_2$ dispersion on catalytic activity might not be significant among the catalysts for R > 3. For the catalyst with the lowest R (= 3), Raman spectra (Fig. 3) indicated low dispersion of the catalytically active phase, and this low dispersion is likely related to the pore plugging suggested by the significant decrease in PV (Fig. 2).

### 3.2. Catalytic activity

Table 3 shows the results of the catalytic activity tests for HDS of thiophene. The catalytic activity increased with increasing R up to R = 8 and then decreased for R > 9. The activity for the prepared catalysts with hydrolysis ratio R = 8 ~ 9 ($126.10^{-9}$ $mol.g^{-1}.s^{-1}$) was similar to that for the reference industrial catalyst ($135.10^{-9}$ $mol.g^{-1}.s^{-1}$). Taking into account that the Mo loading on the prepared catalysts (10 wt% Mo) was lower than that on the reference industrial catalyst (15 wt% Mo), the specific catalytic activity for most of the prepared catalysts was higher than that of the reference industrial catalyst. This suggests that the dispersion and structure of the catalytically active phase were optimized on these prepared catalysts.

The selectivity to butane (Table 3) increased with increasing R up to R = 7 and then remained constant with further increases in R. The reaction mechanisms in the HDS of thiophene have been extensively investigated [60-62]. According to the most recent report [62], butane would not be produced by the hydrogenation of 1-butene as the final step of a sequential reaction, but would be produced in parallel with 1-butene from the adsorbed $C_4H_9S$. Although the catalytic selectivity should be compared at the same conversion, the results in Table 3 suggest that the catalysts prepared with R > 6 have

higher hydrogenation activity than those with R = 3 ~ 6.

Table 4 shows the results of the catalytic activity tests for HDS of DBT. The catalytic activity increased with increasing R up to R = 10 and then decreased for R > 10. The highest activity was observed for R = 10 and 11, in contrast to maxima at R = 8 and 9 observed for HDS of thiophene. In general, the HDS of DBT as a function of R is similar to that for HDS of thiophene. The activity levels for the prepared catalysts with hydrolysis ratio R > 5 were higher than that of the reference industrial catalyst, even when one ignores the difference in loading of the catalytically active phase. The major reaction product for all the prepared catalysts was biphenyl (BP), whose yield was about 90 ± 5%. This high selectivity to BP indicates that, irrespective of R, the catalytic feature of the prepared catalysts was direct desulfurization (DDS)-oriented (represented here by 4,6-DMDBT HDS in Fig. 6). Note that the reference industrial catalyst exhibited lower selectivity for BP (about 76 %) and higher selectivity for cyclohexylbenzene (CHB) (about 23 %) compared with the values for the prepared catalysts; namely, the reaction over the reference industrial catalyst was more hydrogenation (HYD)-oriented than that over the prepared catalysts.

Table 5 shows the results of the catalytic activity tests for HDS of 4,6-DMDBT. The R dependence of the catalytic activity showed a trend similar to that for HDS of thiophene and DBT. However, the superiority of the prepared catalysts to the reference industrial catalyst was almost eliminated in the HDS of 4,6-DMDBT. In fact, the highest HDS rate of the prepared catalyst observed for R = 9 was comparable to that of the reference industrial catalyst. Even when the catalytic activity was compared on a per-Mo-gram basis, the activity of the prepared catalysts was lower than that of the reference industrial catalyst except for R = 9 and 10.

The main reaction product after removal of sulfur was 3,3'-dimethylcyclohexylbenzene (3,3'-DMCHB) for all the prepared and reference industrial catalysts, and the yield of 3,3'-dimethylbiphenyl (DMBP) was much smaller than that of 3,3'-DMCHB (Table 5). The cracked products observed for R = 7 ~ 10 (6.8 ~ 11.3 %) were mainly methylcyclohexane and toluene in equivalent proportions. As reported by Bataille *et al.* [63], this equimolarity indicates that methylcyclohexane and toluene were formed by the cracking of 3,3'-DMCHB; if 3,3'-DMBP were cracked, the toluene / methylcychlohexane ratio would be much higher than 1 [63] (see Fig. 6). The low selectivity to 3,3'-DMCHB was due to the steric hindrance caused by two methyl groups [64,65], which reduced the DDS reaction rate of 4,6-DMDBT over both the prepared and reference industrial catalysts. Because sulfur removal from 4,6-DMDBT is facilitated when it is preceded by the hydrogenation of an aromatic ring [64,65], the HYD route was the major pathway for the HDS of 4,6-DMDBT.

The catalysts with high HDS activity (*i.e.*, prepared catalysts with R = 7 ~ 10 and the reference industrial catalyst) exhibited lower selectivity for tetrahydro-dimethyldibenzothiophene (4H-DMDBT) compared with the other catalysts (*i.e.*, prepared catalysts with R = 3 ~ 6 and 13) (Table 5). This lower selectivity indicates that over the catalysts with high HDS activity for 4,6-DMDBT, 4H-DMDBT was readily hydrogenated to hexahydro-dimethyldibenzothiophene (6H-DMDBT), which in turn was also readily subject to sulfur removal and was desulfurized to 3,3'-DMCHB. In contrast, the prepared catalysts with low HDS activity for 4,6-DMDBT possessed low activity for the hydrogenation of 4H-DMDBT (Path B in Fig. 6). In addition, the prepared catalysts with R = 7 ~ 10 possessed higher cracking activity compared with the reference industrial catalyst (Table 5).

In summary, (a) for most values of R, the prepared catalysts were superior to the reference industrial catalyst in the HDS of DBT; (b) for R = 8 and 9, the prepared catalysts were comparable to the reference industrial catalyst in the HDS of thiophene; and (c) even the prepared catalyst with the highest activity for the HDS of 4,6-DMDBT was not superior compared with the reference catalyst. This difference in catalytic behavior was likely due to the strong DDS oriented character of the prepared catalysts. Independent of the reactants, the highest activity was observed for catalysts with R = 8 and 9, whereas the lowest activity was observed for R = 3.

## 4. Discussion

### 4.1. Effect of morphology of active phase on catalytic performance

TEM observation (Figs. 4 and 5) and Raman spectroscopy (Fig. 3) reveal high dispersion of the catalytically active phase on all the prepared catalysts except on the catalyst with R = 3. Catalytically active sites of $MoS_2$-based catalysts are located on the edges of $MoS_2$ crystallites regardless of the presence of Co [66-69], although the actual nature of the active phase remains controversial [59,70]. Kasztelan *et al.* [71] reported homothetic growth of $MoS_2$ slabs on supports when the Mo loading was increased, and claimed that the corner sites are not active. Based on these hypotheses, Kasztelan *et al.* explained why a volcano-shaped curve is obtained when plotting HDS activity as a function of Mo loading. According to their conclusion, the maximum HDS activity occurs for slabs containing roughly 20 to 40 Mo atoms, corresponding to a crystallite size between *approx.* 1.5 and 2 nm. In the present study, the observed average slab length of $MoS_2$ crystallites was about ± 1.5 nm (Fig. 4), which is lower than typical values reported in the literature [47] and falls in the optimum range of the slab sizes according

to Kasztelan *et al.* [71]

Another effect of morphology on the catalytic performance is the aspect ratio, which is defined as the number of stacked $MoS_2$ slabs divided by the $MoS_2$ slab length. Daage *et al.* [72] developed a model from data on bulk $MoS_2$ and hypothesized that HYD active sites are located only on the top and bottom planes of $MoS_2$ slabs, which they called "rim" sites, whereas DDS active sites are on all the edge sites. As evidenced by the TEM observation in Fig. 5, most of the $MoS_2$ slabs in the prepared catalysts in our current study were single- or two-layered slabs. Furthermore, the fractal geometry inherent to the sol-gel prepared $Al_2O_3$ support [46] likely reduces the steric hindrance that would decrease the HYD route on the edge sites. Despite the HYD-oriented morphology [72] obtained from the above TEM observation, all the prepared catalysts exhibited higher DDS-oriented characteristics compared with those of the reference industrial catalyst for both DBT (Table 4) and 4,6-DMDBT (Table 5).

Thus, the morphology of $MoS_2$ slabs on the sol-gel prepared $Al_2O_3$ was optimized toward the HDS reaction except for the catalyst with R = 3 for which an undesirable oxidic precursor, $CoMoO_4$, was observed. For R > 3, no evident difference in the morphology of $MoS_2$ slabs was observed among the prepared catalysts, namely, the average number of stacked $MoS_2$ slabs was 2 and the average slab size was about 1.5 nm.

4.2. Effect of properties of the supports on catalytic performance

Tables 3-5 reveal that the HDS activities were the highest for the prepared catalysts with hydrolysis ratio R = 9 and 10, which possessed relatively large pores (Table 2). In fact, the HDS reaction rate of thiophene increased linearly with increasing average PD

when $2.5 \leq PD \leq 6$ nm (Fig. 7), and was relatively constant when PD > 6 nm. This indicates that the HDS reaction of thiophene was controlled to a certain extent by the pore diffusional limitation [73] in catalysts with PD < 6 nm.

Figure 8 shows the HDS reaction rate of DBT as a function of average PD. Similar to the relationship for HDS of thiophene (Fig. 7), the reaction rate of DBT increased linearly with increasing PD when $2.5 \leq PD \leq 6$ nm, and was relatively constant when PD > 6 nm. Figure 8 also shows the ratio of the HDS reaction rate of DBT relative to that of thiophene. This relative ratio decreased relatively linearly with increasing PD, indicating that the catalytically active sites for both of the HDS reactions were the same. The slightly negative slope suggests that the effect of the pore diffusional limitation on the HDS of thiophene was similar to or slightly larger than that on HDS of DBT. According to mass transfer theory [73], the effect of the pore diffusional limitation on the reaction rates is governed by many factors, not only by the pore diameter or the reactant molecular size but also by the catalyst particle size and intrinsic reaction rates. Therefore, it is not appropriate to quantitatively discuss here the effect of the pore diffusional limitation on the HDS reaction rates. Qualitatively, however, considering that the molecular size of thiophene and DBT (0.5 nm) was sufficiently smaller than the average PD of the present prepared catalysts, the pore diffusion was likely suppressed by the small mouths of ink-bottle type pores that were characteristic to the sol-gel prepared $Al_2O_3$ powders with R < 8 and R > 10.

Figure 9 shows the HDS reaction rates of 4,6-DMDBT as a function of the average PD. The rate increased linearly with increasing PD up to PD = 5 nm, similar to the relationships observed for the reactions of thiophene and DBT (Figs. 7 and 8,

respectively). The catalysts with PD > 6 nm exhibited significantly higher activity than that expected from the extrapolation of the relationship obtained for the catalysts with PD < 5 nm. This significant increase in activity for catalysts with PD > 6 nm might be partly due to the molecular size of 4,6-DMDBT (0.6 nm) being larger than that of either thiophene or DBT; the methyl groups of 4,6-DMDBT increase the cross-section of the molecule by about 15 % compared with the cross-section for DBT. This difference in cross-section, however, is not large enough to explain the difference in catalytic performance, because the average PD of the prepared catalysts is almost 10 times larger than the cross-section of the molecules. Thus, some other major factor is responsible for the difference in the catalytic performance.

The prepared catalysts with low HDS activity for 4,6-DMDBT also showed low HYD activity for 4H-DMDBT (Step B in Fig. 6), as discussed in § 3.2. Figure 10 shows evidence that HYD of 4H-DMDBT is essential for the HDS of 4,6-DMDBT via the predominant HYD route. Namely, the catalysts with R = 7 ~ 10, particularly those with R = 9 and 10, possessed higher HYD activity for olefins compared with the other prepared catalysts.

The $Al_2O_3$ supports with hydrolysis ratio R = 7~ 10 possessed a higher ratio of strong acid sites compared with other supports (Table 1). Therefore, the high HYD activity of the catalysts with R = 7 ~ 10 was likely related to the acidity of the $Al_2O_3$ supports. Furthermore, previous SEM observation [46] revealed that $Al_2O_3$ powders with R = 9 and 10 have a “cloudy structure” not observed in other $Al_2O_3$ powders. This cloudy structure results in “pseudo-cylindrical” pores and a high ratio of strong acid sites. In conclusion, the $Al_2O_3$ powders prepared with R = 7 ~ 10, particularly R = 9 and 10, possessed pseudo-cylindrical pores and strong acidity, both of which were favorable for the HDS of

4,6-DMDBT, although the acid sites yielded undesirable cracking compounds as shown in Table 5.

Despite their HYD-oriented morphology, the prepared catalysts exhibited a higher DDS-oriented catalytic functionality compared with the reference industrial catalyst (Table 4). The HYD activity of the reference industrial catalyst was probably enhanced by a specific proprietary additive. Because the reference industrial catalyst was developed particularly for deep HDS of diesel fuel fractions, the additive was probably designed to increase the HYD activity without increasing the cracking activity of the catalysts. This suggests that the HDS activity of the prepared catalysts can be increased by certain additives, such as zeolites or elements that moderately increase the acidity of the catalysts.

## 5. Summary

This study revealed the following characteristics of CoMo catalysts supported on sol-gel-prepared $Al_2O_3$.

1. Co and Mo loading decreased the pore volume and pore diameter of the catalysts. The average pore diameter of the prepared catalysts with hydrolysis ratio R > 6 was about 6 nm, whereas that of catalysts with R = 3 and 4 was smaller than 4 nm. Pore plugging during the catalyst preparation supposedly caused these small average pore diameters.
2. The catalytically active phase, Co-promoted $MoS_2$, was highly dispersed as single- or two-layered slabs with average length of *approx.* 1.5 nm except for a catalyst supported on the $Al_2O_3$ with the lowest R (= 3) for which the presence of bulk $CoMoO_4$ was clearly evidenced.

3. The catalysts prepared with hydrolysis ratio R = 7 ~ 10 exhibited higher HDS activity for all three reactants tested (DBT, thiophene, and 4,6-DMDBT) compared with the other prepared catalysts (*i.e.*, R < 7 and R > 10). Such higher activity was mainly due to the large pore diameters (*ca.* 6 nm) of these catalysts with R = 7 ~ 10. The effect of the pore diffusional limitation was more significant than expected due to the ink-bottle shape of the sol-gel-prepared $Al_2O_3$.
4. For thiophene, the activity of the prepared catalysts with hydrolysis ratio R = 8 and 9 was similar to that of the reference industrial catalyst, and for DBT the HDS activity of the prepared catalysts with R = 6 ~ 13 was higher than that of the reference industrial catalyst. This was due to the high catalyst dispersion (see characteristic 2 above in this Summary). For 4,6-DMDBT, however, the HDS activity of the prepared catalysts was lower than that of the reference industrial catalyst. Among the prepared catalysts, relatively high 4,6-DMDBT HDS activity was observed for the catalysts with R = 9 and 10. This was due to the cylindrical pore shape and higher proportion of strong acidity of these catalysts. The cylindrical pore shape increased the pore diffusion of large 4,6-DMDBT molecules and the high proportion of strong acidity enhanced the HYD function that was essential for the HDS of 4,6-DMDBT. Finally, the results for the 4,6-DMDBT HDS activity and selectivity suggest that olefin hydrogenation function is required for the HDS of 4,6-DMDBT.

**Acknowledgements**

The authors thank the Science and Technology Agency (STA), which funded this work through the Japan Society for Promotion of Science (JSPS).

**References**


1. European Directive 98/70/CE, 1998.

2. X. Ma, K. Sakanishi, I. Mochida, Ind. Eng. Chem. Res. 33 (1994) 218.

3. S. Shih, S. Mizrahi, L. A. Green, M. S. Sarli, Ind. Eng. Chem. Res. 31 (1992) 232.

4. T. Kabe, A. Ishihara, H. Tajima, Ind. Eng. Chem. Res. 31 (1992) 1577.

5. D. D. Whitehurst, T. Isoda, I. Mochida, Adv. Catal. 42 (1998) 345.

6. M. Vrinat, M. Lacroix, M. Breysse, L. Mosoni, M. Roubin, Catal. Lett. 3 (1989) 405.

7. A.P. Raje, S.-J. Liaw, B.H. Davis, Appl. Catal. 150 (1997) 297.

8. A.P. Raje, S.-J. Liaw, R. Srinivasan, B.H. Davis, Appl. Catal. 150 (1997) 319.

9. T. A. Pecoraro, R. R. Chianelli, J. Catal. 67 (1981) 430.

10. M. Lacroix, N. Boutarfa, C. Guillard, M. Vrinat, M. Breysse, J. Catal. 120 (1989) 473.

11. J. Shabtai, N.K. Nag, F.E. Massoth, J. Catal. 104 (1987) 413.

12. J.A. De Los Reyes, M. Vrinat, C. Geantet, M. Breysse, Catal. Today 10 (1991) 645.

13. K. Lu, Y.J. Kuo, B.J. Tatarchuk, J. Catal. 116 (1989) 373.

14. A. Ishihara, M. Nomura, T. Kabe, J. Catal. 150 (1994) 212.

15. A. Ishihara, J. Lee, F. Dumeignil, R. Higashi, A. Wang, E.W. Qian, T. Kabe, J. Catal. 217 (2003) 59.

16. A. Ishihara, J. Lee, F. Dumeignil, E.W. Qian, T. Kabe, J. Catal. 224(2) (2004) 243.

17. J. Lee, A. Ishihara, F. Dumeignil, E.W. Qian, T. Kabe, J. Mol. Cat. 213(2) (2004) 207.

18. J. Lee, A. Ishihara, F. Dumeignil, M. Kou, O. Yuji, E.W. Qian, T. Kabe, J. Mol Cat. 209(1-2) (2004) 155.

19. A. Ishihara, J. Lee, F. Dumeignil, E.W. Qian, T. Kabe, Proceedings of the 13th International Congress on Catalysis (2004).

20. A. Ishihara, J. Lee, F. Dumeignil, E.W. Qian, T. Kabe, Proceedings of the 10th APPChE Congress (2004).

21. A.M. Venezia, V. La Parola, G. Deganello, B. Pawelec, J.L.G. Fierro, J. Catal. 215 (2003) 317.

22. Y. Ogawa, M. Toba, Y. Yoshimura, Appl. Catal. A: Gen. 246(2) (2003) 213.

23. T. Fujikawa, K. Idei, K. Ohki, H. Mizuguchi, K. Usui, Appl. Catal. A: Gen. 205 (2001) 71.

24. D. Wang, X. Li, E.W. Qian, A. Ishihara, T. Kabe, Appl. Catal. A: Gen. 238(1) (2002) 109.

25. D. Wang, W. Qian, A. Ishihara, T. Kabe, Appl. Catal. A:Gen. 224(1-2) (2002) 191.

26. T. Klimowa, D.S. Casados, J. Ramírez, Catal. Today 43(1-2) (1998) 135.

27. J. Trawczyński, J. Walendziewski, Appl. Catal. A: Gen. 119(1) (1994) 59.

28. V.L. Barrio, P.L. Arias, J.F. Cambra, M.B. Güemez, B. Pawelec, J.L.G. Fierro, Fuel 82(5) (2003) 501.

29. J. Ramirez, S. Fuentes, G. Diaz, M. Vrinat, M. Breysse, M. Lacroix, Appl. Catal. 52 (1989) 211.

30. Y. Okamoto, A. Maezawa, T. Imanaka, J. Catal. 120 (1989) 29.

31. E. Olguin, M. Vrinat, L. Cedeño, J. Ramirez, M. Borque, A. López-Agudo, Appl.

Catal. A 165 (1997) 1.

32. J. Ramirez, L. Ruiz-Ramirez, L. Cedeno, V. Harle, M. Vrinat, M. Breysse, Appl. Catal. A 93 (1993) 163.

33. J. Ramirez, A. Gutierrez, J. Catal 170 (1997) 108.

34. E. Lecrenay, K. Sakanishi, T. Nagamatsu, I. Mochida, T.Suzuka, Appl. Catal. B 18 (1998) 325.

35. S. Yoshinaka, K. Segawa, Catal. Today 45 (1998) 293.

36. Z. B. Wei, C. D. Wei, Q. Xin, Acta Physico-chemica Sinica 10 (1994) 402.

37. Z. B. Wei, Q. Xin, X. X Guo, P. Grange, B. Delmon, S. Yoshida, Catal. Sci. Technol. 1 (1991) 147.

38. C. Pophal, F. Kameda, K. Hoshino, S. Yoshinaka, K. Segawa, Catal. Today 39 (1997) 21.

39. A. Ishihara, D.H. Wang, E.W. Qian, T. Kabe, Proceedings of the 226$^{th}$ ACS National Meeting 48(2) (2003) 607.

40. D.H. Wang, E.W. Qian, A. Ishihara, T. Kabe, J. Catal. 209 (2002) 266.

41. D.H. Wang, E.W. Qian, A. Ishihara, T. Kabe, J. Catal. 203 (2001) 322.

42. A. Ishihara, F. Dumeignil, D. Wang, X. Li, H. Arakawa, E.W. Qian, S. Inoue, A. Muto, T. Kabe, J. Jpn. Petrol. Inst. 48(1) (2005) 37.

43. B. Pawelec, R. Mariscal, J.L.G. Fierro, A. Greenwood, P.T. Vasudevan, Appl. Catal. A: Gen. 206(2) (2001) 295.

44. M. Sugioka, F. Sado, T. Kurosaka, X. Wang, Catal. Today 45 (1998) 327.

45. F. Dumeignil, J. Grimblot, in G.F. Froment, P. Grange (Ed.), Hydrotreatment and Hydrocracking of Oil Fractions, B. Delmon, 1999, p. 357.

46. F. Dumeignil, K. Sato, M. Imamura, N. Matsubayashi, E. Payen, H. Shimada, Appl. Catal. A: Gen. 241(1-2) (2003) 319.

47. E. Payen, R. Hubaut, S. Kasztelan, O. Poulet, J. Grimblot, J. Catal. 147(1) (1994) 123.

48. E. Payen, M. C. Dhamelincourt, P. Dhamelincourt, J. Grimblot, J. P. Bonnelle, Appl. Spectr. 36(1) (1982) 30.

49. N. Y. Topsøe, H. Topsøe, J. Catal. 75 (1982) 354.

50. P. Dufresne, E. Payen, J. Grimblot, J. - P. Bonnelle, J. Phys. Chem. 85 (1981) 2344.

51. S. Kasztelan, E. Payen, H. Toulhoat, J. Grimblot, J. - P. Bonnelle, Polyhedron 5(1/2) (1986) 157.

52. H. Shimada, N. Matsubayashi, T. Sato, Y. Yoshimura, A. Nishijima, J. Catal. 138 (1992) 746.

53. E. Payen, S. Kasztelan, Trends in Physical Chemistry 4 (1994) 363.

54. Y. Tanaka, H. Shimada, N. Matsubayashi, A. Nishijima, M. Nomura, Catal. Today 45 (1998) 319.

55. G. Plazenet, S. Cristol, J.F. Paul, E. Payen, J. Lynch, Phys. Chem. Chem. Phys. 3 (2001) 246.

56. P. Da Silva, N. Marchal, S. Kasztelan, Stud. Surf. Sci. Catal. 106 (1997) 353.

57. S. Srinivasan, A.K. Datye, C.H.F. Peden, J. Catal. 137 (1992) 513.

58. C. Calais, N. Matsubayashi, C. Geantet, Y. Yoshimura, H. Shimada, A. Nishijima, M. Lacroix, M. Breysse, J. Catal. 174 (1998) 130.

59. Y. Iwata, Y. Araki, K. Honna, Y. Miki, K. Sato, H. Shimada, Catal. Today 65 (2001) 335.

60. P. Kieran, C. Kemball, J. Catal. 4 (1965) 394.

61. J. M. J. G. Lipsch, C. G. C. A. Schuit, J. Catal. 15 (1969) 179.

62. D. L. Sullivan, J. G. Ekerdt, J. Catal. 178 (1998) 226.

63. F. Bataille, J.L. Lemberton, G. Pérot, P. Leyrit, T. Cseri, N. Marchal, S. Kasztelan, Appl. Catal. A: Gen. 220 (2001) 191.

64. M. Houalla. N. K. Nag, A. V. Sapre, D. H. Broderick, B. C. Gates, AIChE J. 24 (1978) 1015.

65. M. Houalla, D. H. Broderic, A. V. Sapre, N. K. Kag, V. H. J. de Beer, B. C. Gates, H. Kwart, J. Catal. 61 (1980) 523.

66. I. Alstrup, I. Chorkendorff, R. Candia, B.S. Clausen, H. Topsøe, J. Catal. 77 (1982) 397.

67. S. Houssenbay, S. Kasztelan, H. Thouloat, J.-P. Bonnelle, J. Grimblot, J. Phys. Chem. 93 (1989) 7176.

68. S. Harris, Polyhedron 5 (1986) 151.

69. L. Blanchard, J. Grimbot, J.-P. Bonnelle, J. Catal. 98 (1986) 229.

70. S. Eijbouts, J.J.L. Heinerman, H.J.W. Elzerman, Appl. Catal. A: Gen. 105 (1993) 53.

71. S. Kaztelan, H. Toulhoat, J. Grimblot, J. P. Bonnelle, Appl. Catal. 13 (1984) 127.

72. M. Daage, R. E. Chianelli, J. Catal. 149 (1994) 414.

73. C. N. Satterfield, Mass transfer in heterogeneous catalysis, Cambridge, Mass., M.I.T. Press, 1969.

74. C. Mauchaussé, PhD Thesis, Lyon (1988).

75. G. Pérot, Catal. Today 86 (2003) 111.

## Figure captions

Figure 1. HDS activity of DBT over a prepared catalyst with hydrolysis ratio R = 8.

Figure 2. Average pore diameter (PD) and relative pore volume (PV) of oxidic precursors of prepared catalysts as a function of hydrolysis ratio R.

Figure 3. Raman spectra of oxidic precursors of prepared catalysts.

Figure 4. Distribution of $MoS_2$ slab length on prepared catalysts with hydrolysis ratio R=5, 10, and 11. Distribution analysis was done using the method by Mauchaussé [74].

Figure 5. Distribution of number of stacked $MoS_2$ layers on prepared catalysts. Distribution analysis was done using the method by Mauchaussé [74].

Figure 6. HDS reaction scheme of 4,6-DMDBT (adapted from Ref. 75).

Figure 7. HDS activity for thiophene as a function of average pore diameter (PD) of prepared catalysts and reference industrial catalyst.

Figure 8. HDS activity for DBT as a function of average pore diameter (PD) of prepared catalysts and reference industrial catalyst.

Figure 9. HDS activity for 4,6-DMDBT as a function of average pore diameter (PD) of prepared catalysts and reference industrial catalyst.

Figure 10. HDS activity and selectivity to 4H-DMDBT in the HDS reaction of 4,6-DMDBT for prepared catalysts and reference industrial catalyst.

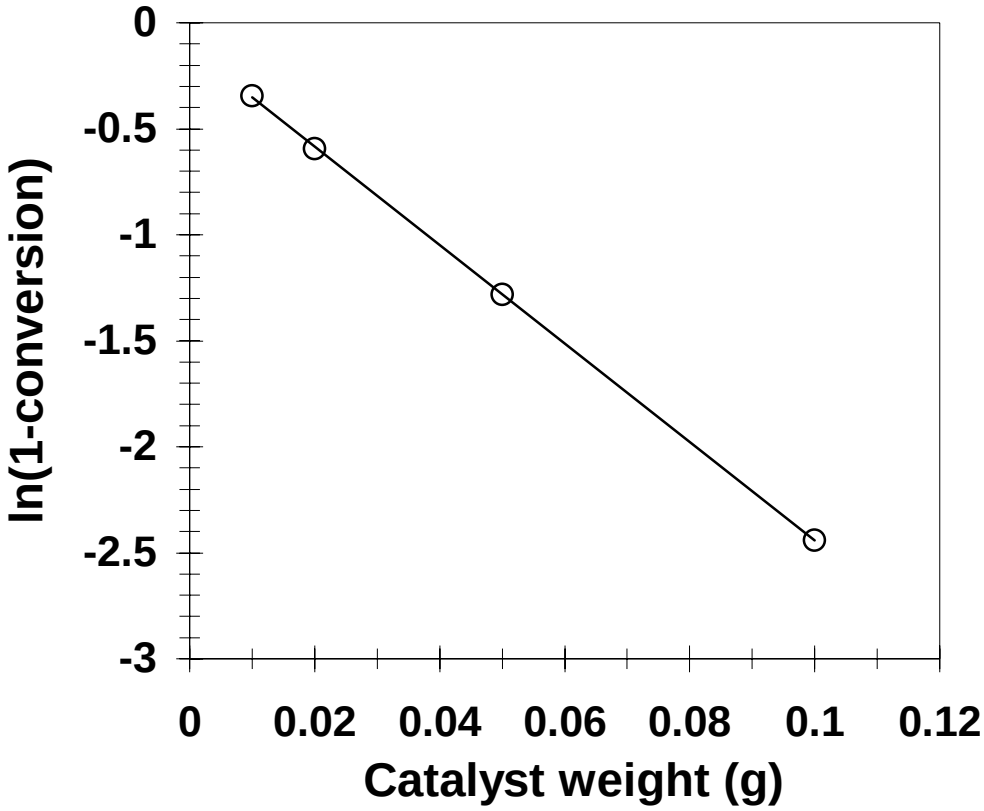
0
-0.5
-1
-1.5
-2
-2.5
-3
ln(1-conversion)
0
0.02
0.04
0.06
0.08
0.1
0.12
Catalyst weight (g)

**Fig. 1**

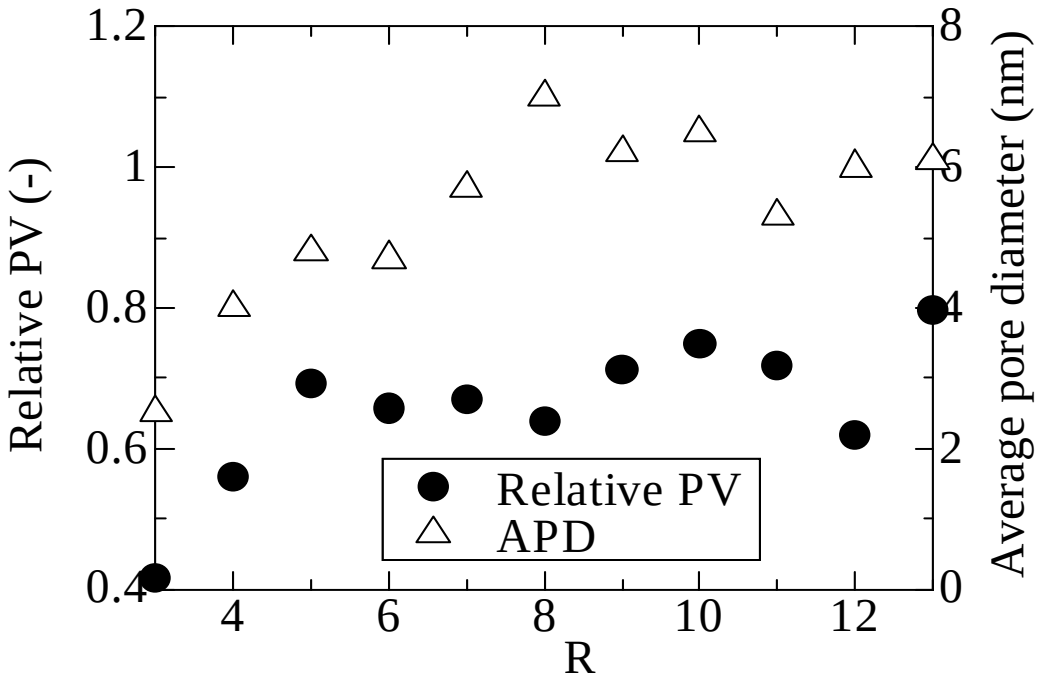
Relative PV (-)
Average pore diameter (nm)
R
Relative PV
APD
1.2
1
0.8
0.6
0.4
8
6
4
2
0
4
6
8
10
12

**Fig. 2**

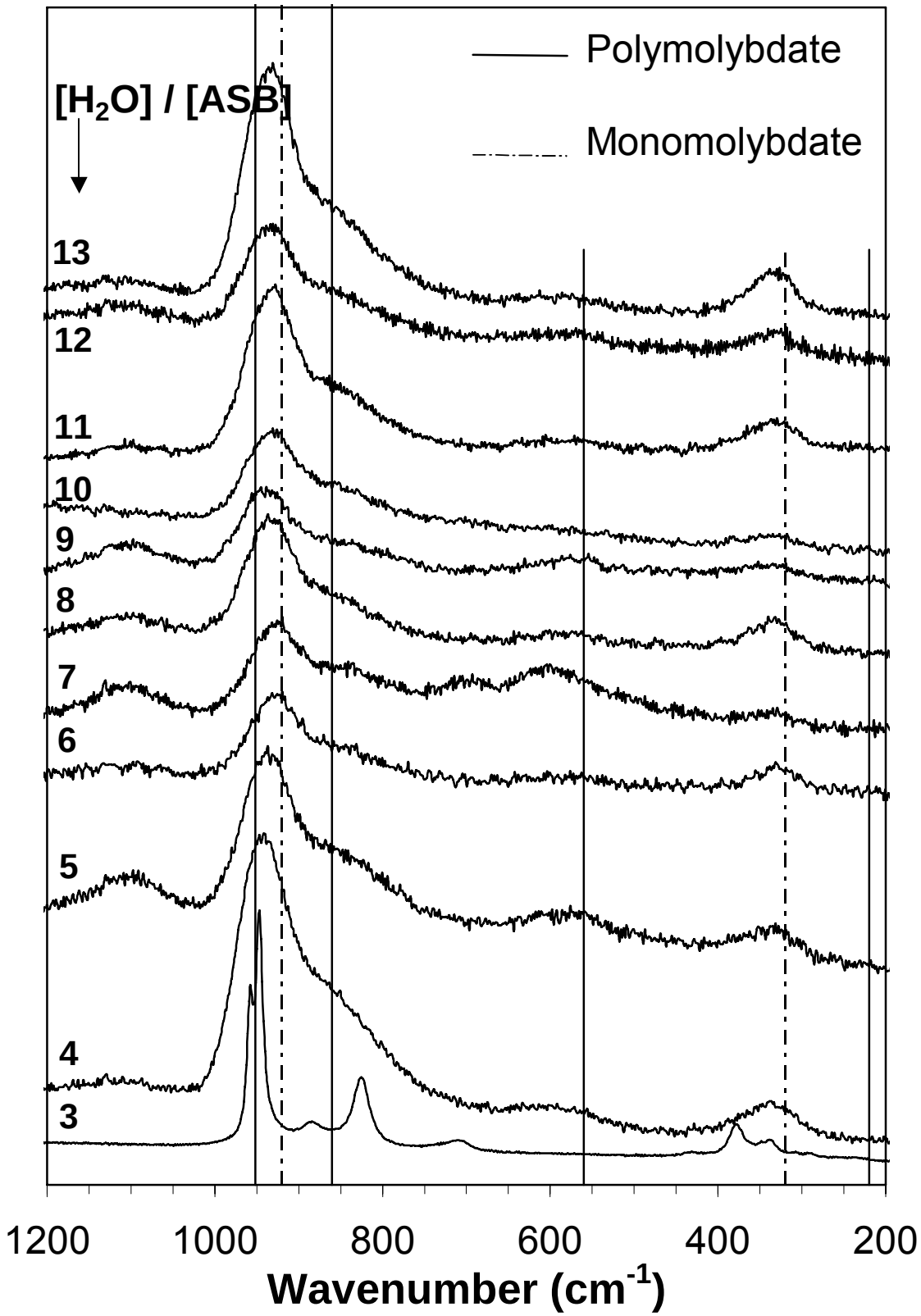
Polymolybdate
Monomolybdate
[H2O] / [ASB]
13
12
11
10
9
8
7
6
5
4
3
1200
1000
800
600
400
200
Wavenumber (cm-1)

**Fig. 3**

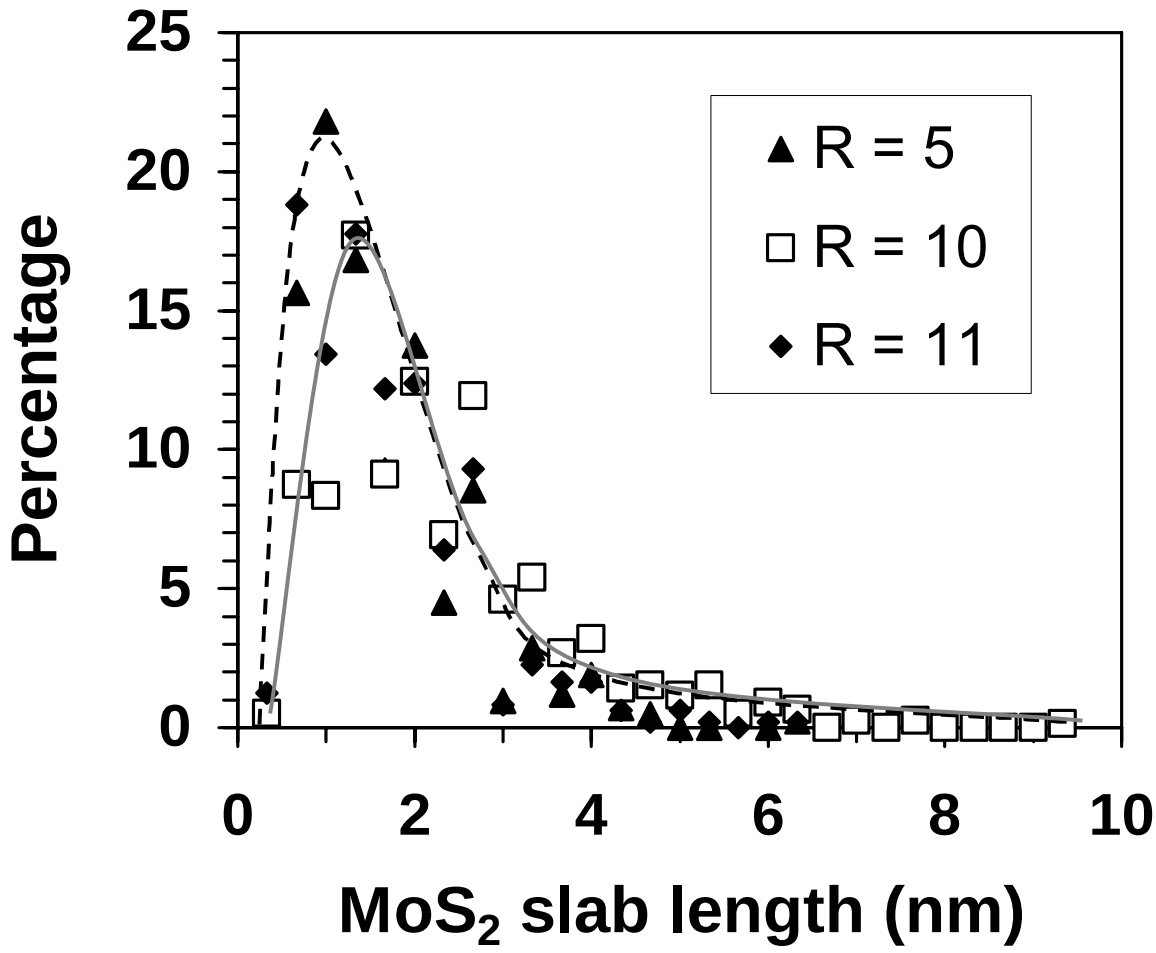
25
20
15
10
5
0
Percentage
R = 5
R = 10
R = 11
0
2
4
6
8
10
MoS2 slab length (nm)

**Fig. 4**

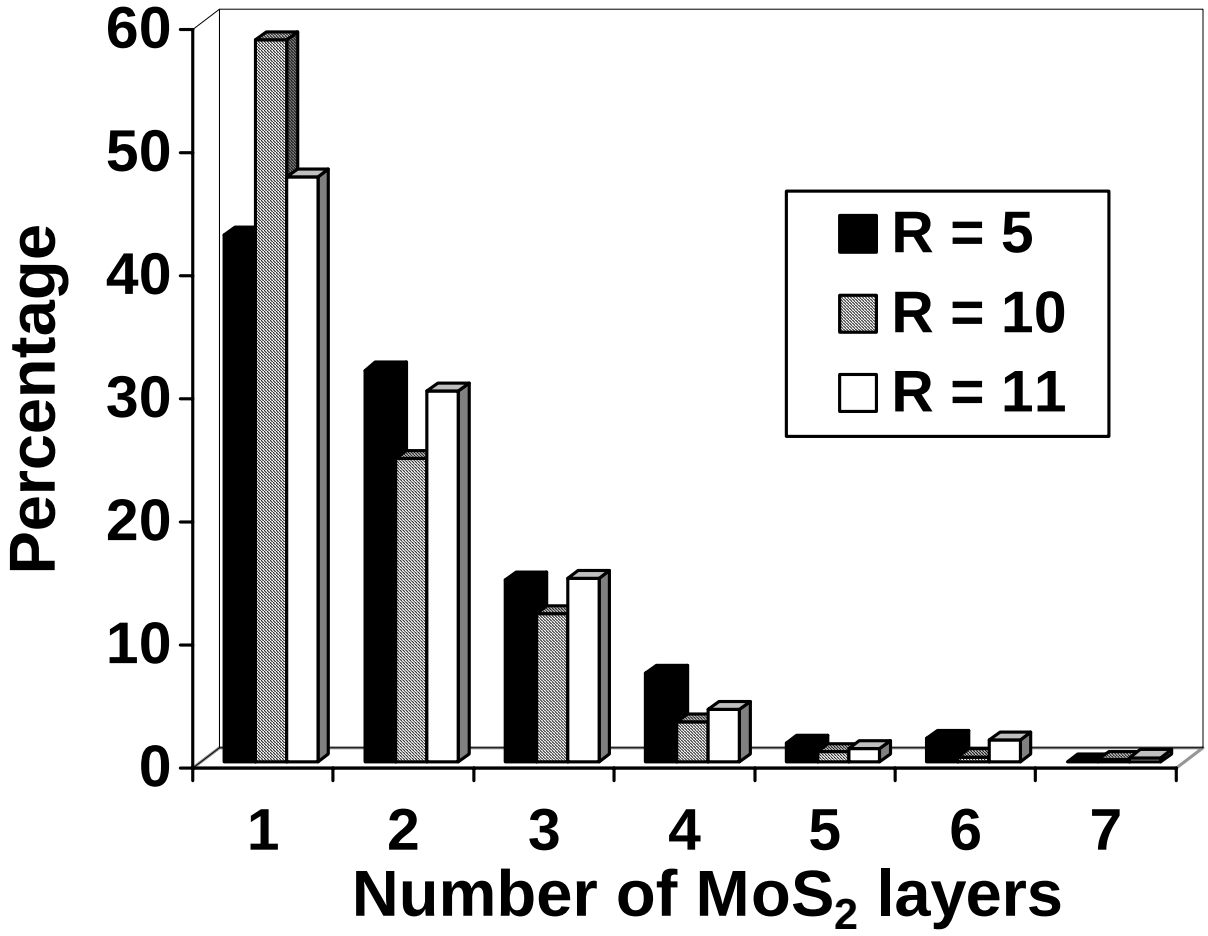
60
50
40
30
20
10
0
Percentage
R = 5
R = 10
R = 11
1
2
3
4
5
6
7
Number of MoS2 layers

**Fig. 5**

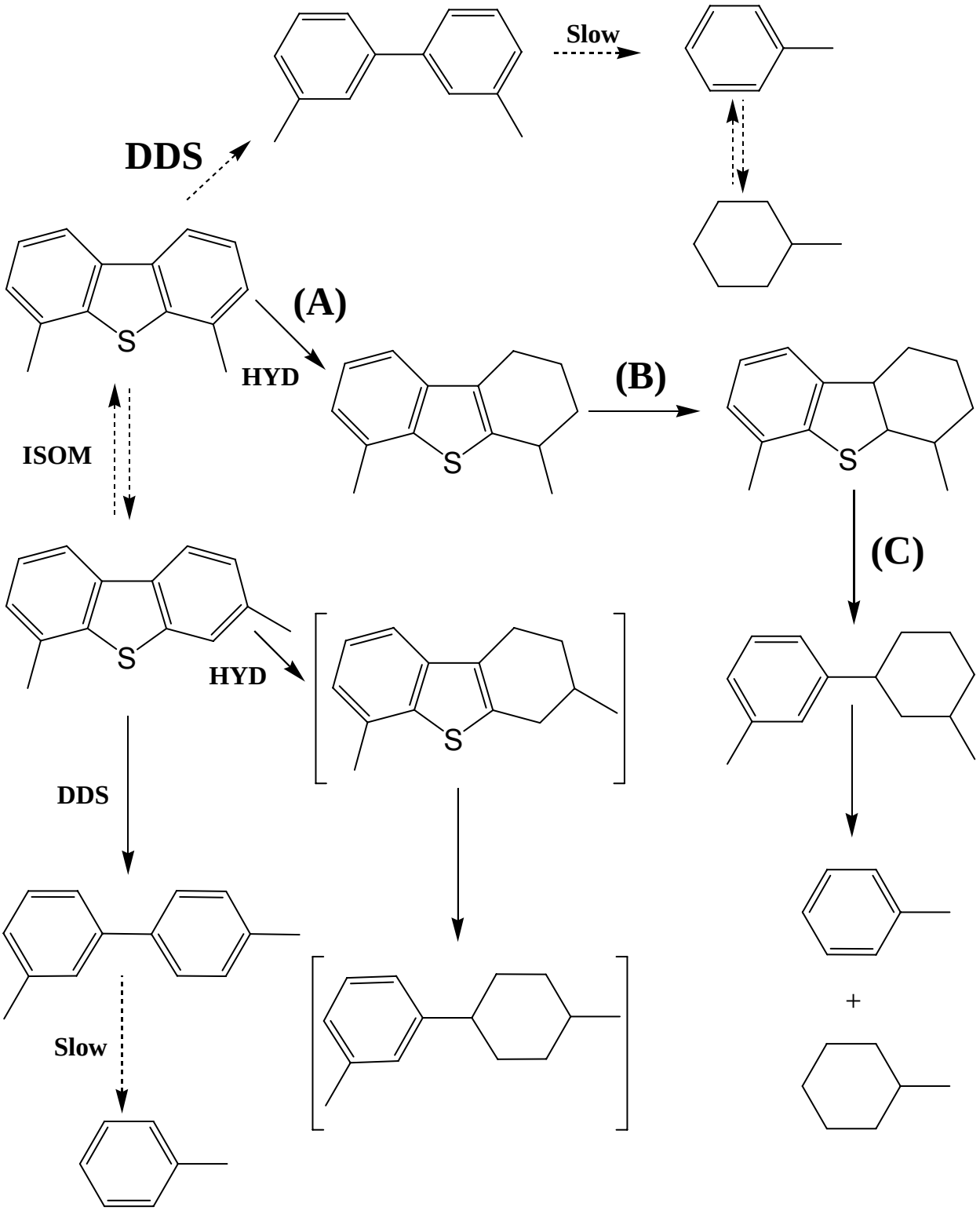


Fig. 6

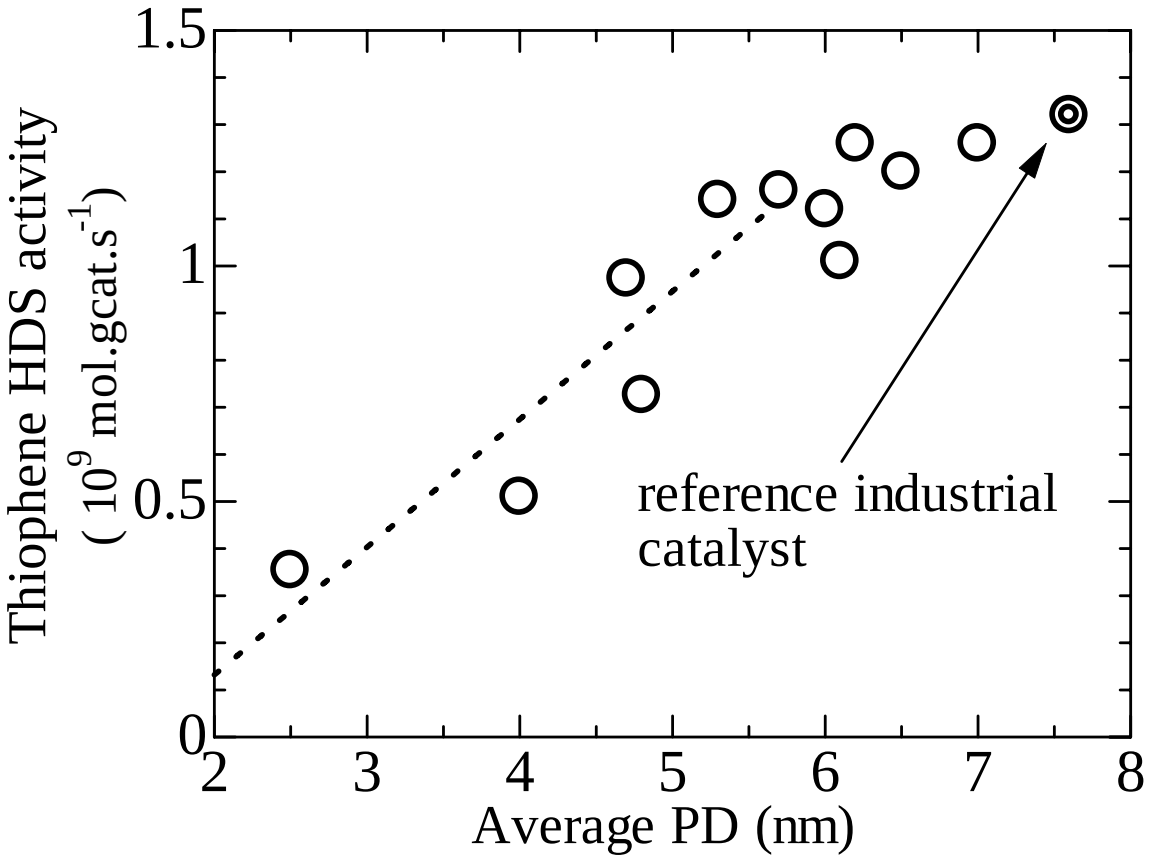
Thiophene HDS activity
( $10^9$ mol.gcat.$s^{-1}$)
1.5
1
0.5
0
2
3
4
5
6
7
8
Average PD (nm)
reference industrial
catalyst

**Fig. 7**

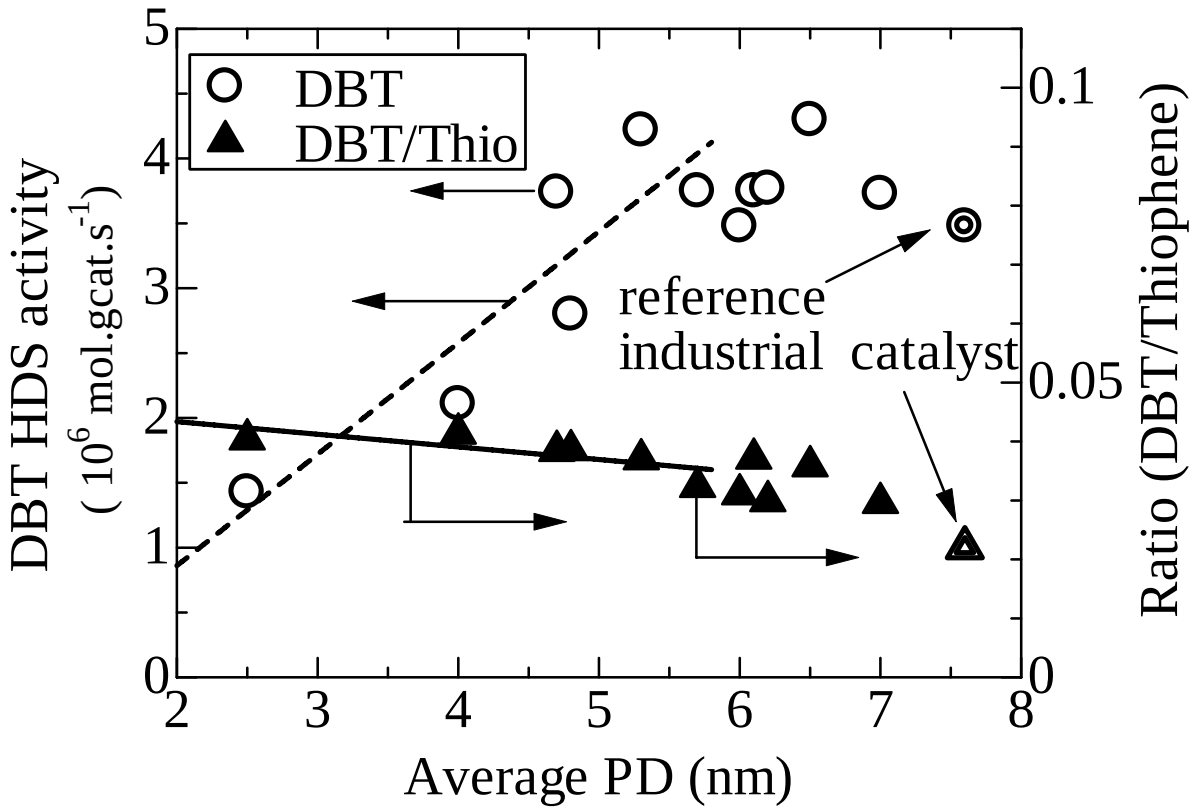
DBT
DBT/Thio
reference
industrial catalyst
DBT HDS activity
( 10^6 mol.gcat.s^-1 )
Ratio (DBT/Thiophene)
Average PD (nm)
0
1
2
3
4
5
0
0.05
0.1
2
3
4
5
6
7
8

**Fig. 8**

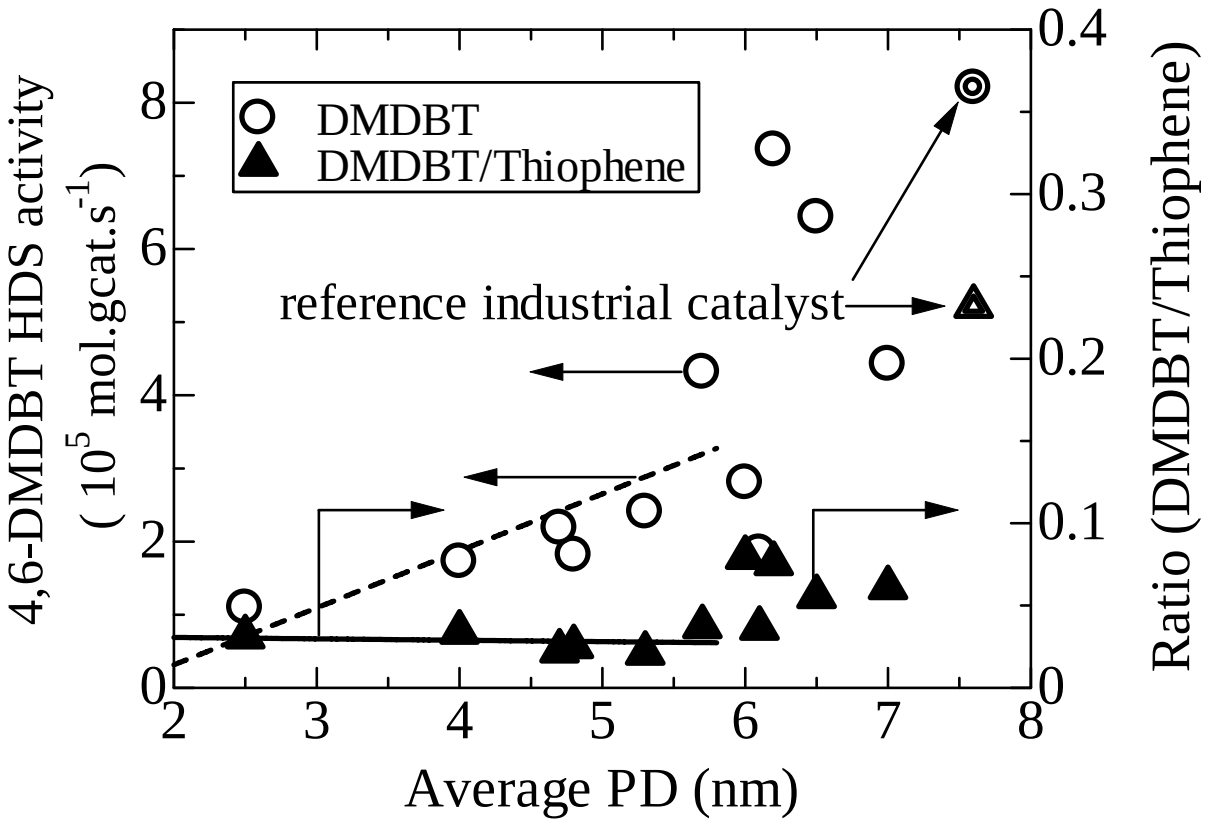
4,6-DMDBT HDS activity
( 10^5 mol.gcat.s^-1 )
Ratio (DMDBT/Thiophene)
Average PD (nm)
DMDBT
DMDBT/Thiophene
reference industrial catalyst
0
2
4
6
8
0
0.1
0.2
0.3
0.4
2
3
4
5
6
7
8

**Fig. 9**

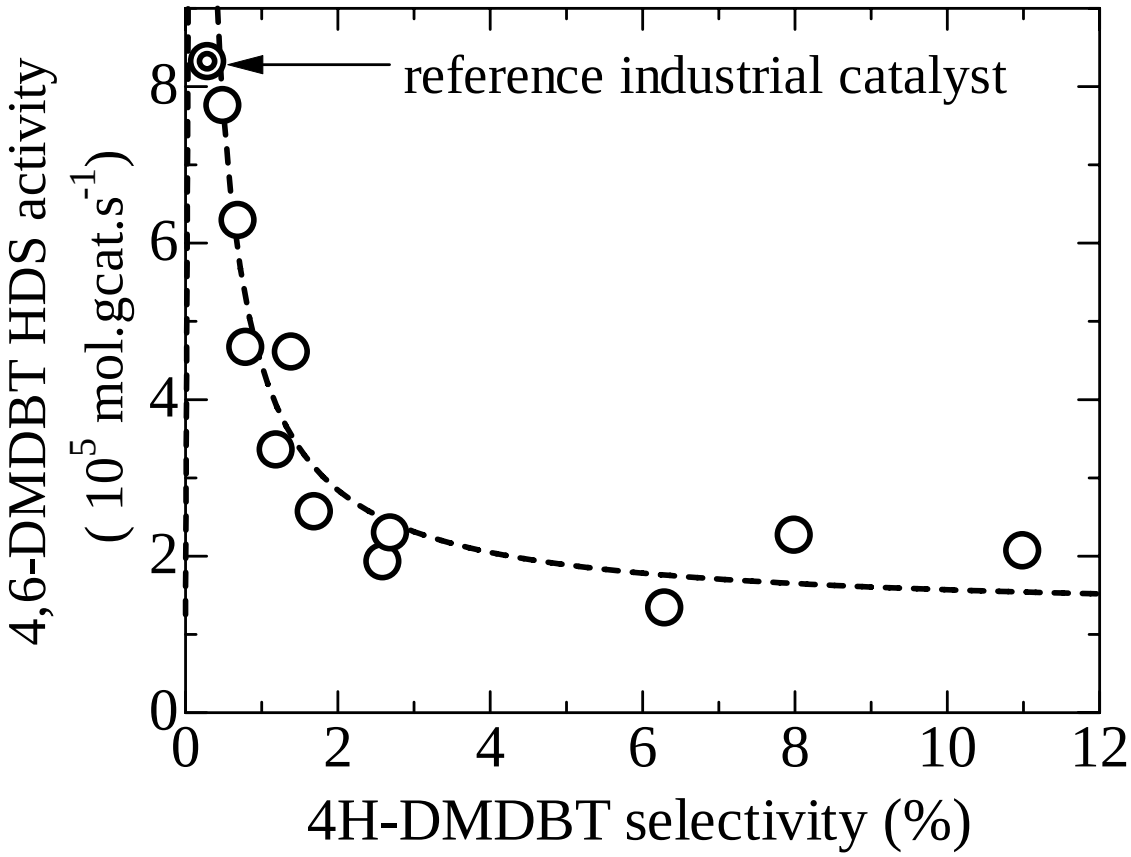
reference industrial catalyst
4,6-DMDBT HDS activity
( 10^5 mol.gcat.s^-1 )
4H-DMDBT selectivity (%)
0
2
4
6
8
10
12

**Fig. 10**

**Table 1** Textural and acidic properties of the sol-gel-prepared $Al_2O_3$ supports

| R | BET Specific Surface Area ($m^2.g^{-1}$) | Water Pore Volume ($cm^3.g^{-1}$) | BJH Pore Volume ($cm^3.g^{-1}$) | Average Pore Diameter* (nm) | Total Acidity** ($mmol.g^{-1}$) | Ratio of Strong Acidity*** (%) |
|---|---|---|---|---|---|---|
| 3 | 439 | 1.0 | 0.41 | 3.7 | 0.97 | 66.2 |
| 4 | 403 | 1.1 | 0.59 | 5.9 | 1.69 | 68.8 |
| 5 | 399 | 1.3 | 0.62 | 6.2 | 1.94 | 66.2 |
| 6 | 492 | 1.5 | 0.70 | 5.7 | 1.91 | 62.4 |
| 7 | 450 | 1.9 | 0.79 | 7.0 | 1.78 | 74.8 |
| 8 | 408 | 1.7 | 0.94 | 9.2 | 1.73 | 75.2 |
| 9 | 358 | 1.9 | 0.80 | 8.9 | 1.92 | 87.2 |
| 10 | 363 | 1.91 | 0.84 | 9.3 | 1.58 | 85.9 |
| 11 | 407 | 1.7 | 0.71 | 7.0 | 1.88 | 64.5 |
| 12 | 450 | 1.6 | 0.84 | 7.5 | 1.87 | 67.7 |
| 13 | 380 | 1.7 | 0.74 | 7.8 | 2.08 | 77.3 |

* Calculated from the BET surface area and BJH pore volume.

** Total amount of adsorbed $NH_3$ on each catalyst.

*** Relative ratio of strong acidity relative to the total acidity. Strong acidity was defined as the area of the high temperature peak at about 523 K.

**Table 2** Physical properties of oxidic precursors

| R | BET Specific Surface Area ($m^2.g^{-1}$) | Ratio** (-) | BJH Pore Volume ($cm^3.g^{-1}$) | Ratio** (-) | Average PD* (nm) |
|---|---|---|---|---|---|
| 3 | 271 | 0.62 | 0.17 | 0.41 | 2.5 |
| 4 | 331 | 0.82 | 0.33 | 0.56 | 4.0 |
| 5 | 357 | 0.89 | 0.43 | 0.69 | 4.8 |
| 6 | 395 | 0.80 | 0.46 | 0.66 | 4.7 |
| 7 | 375 | 0.83 | 0.53 | 0.67 | 5.7 |
| 8 | 347 | 0.85 | 0.60 | 0.64 | 7.0 |
| 9 | 370 | 1.0 | 0.57 | 0.57 | 6.2 |
| 10 | 387 | 1.1 | 0.63 | 0.71 | 6.5 |
| 11 | 385 | 0.95 | 0.51 | 0.72 | 5.3 |
| 12 | 345 | 0.77 | 0.52 | 0.62 | 6.0 |
| 13 | 385 | 1.0 | 0.59 | 0.79 | 6.1 |
| Ref. | 271 | - | - | - | 7.6 |

* Average pore diameter calculated the BET surface area and BJH pore volume.

** Relative ratio relative to that of the corresponding $Al_2O_3$ support.

**Table 3** Catalytic activities in HDS of thiophene

| R | HDS Rate (x $10^9$ mol.gcat.$s^{-1}$) | Product Distribution | | |
|---|---|---|---|---|
| | | Cis-but-2-ene (%) | But-1-ene + Trans-but-2-ene (%) | Butane (%) |
| 3 | 35.4 | 52.9 | 27.6 | 19.5 |
| 4 | 51.0 | 47.3 | 25.7 | 27 |
| 5 | 72.6 | 42.8 | 23.5 | 33.7 |
| 6 | 97.3 | 38.1 | 23.7 | 38.2 |
| 7 | 116 | 37.2 | 22 | 40.8 |
| 8 | 126 | 38 | 20.1 | 41.9 |
| 9 | 126 | 38 | 20.1 | 41.9 |
| 10 | 120 | 40.3 | 18 | 41.7 |
| 11 | 114 | 38.1 | 20.5 | 41.4 |
| 12 | 112 | 38.2 | 20.3 | 41.5 |
| 13 | 101 | 39.3 | 22.6 | 38.1 |
| Ref. | 135 | 39.7 | 21.8 | 38.5 |

**Table 4** Catalytic activities in HDS reactions of DBT

| R | HDS Rate (x $10^6$ mol.gcat$^{-1}$.s$^{-1}$) | Product Distribution | | | |
|---|---|---|---|---|---|
| | | Biphenyl (%) | Cyclohexylbenzene (%) | 4H-DBT* (%) | 6H-DBT**(%) |
| 3 | 1.43 | 85.7 | 9.6 | 4.2 | 0.5 |
| 4 | 2.11 | 88.9 | 7.6 | 3.1 | 0.4 |
| 5 | 2.80 | 84.6 | 13.3 | 1.9 | 0.2 |
| 6 | 3.74 | 92.3 | 4.1 | 3.3 | 0.3 |
| 7 | 3.75 | 91.8 | 6.0 | 2.0 | 0.2 |
| 8 | 3.73 | 90.4 | 7.5 | 1.9 | 0.2 |
| 9 | 3.77 | 89.0 | 9.0 | 1.8 | 0.2 |
| 10 | 4.30 | 90.6 | 7.4 | 1.8 | 0.2 |
| 11 | 4.22 | 88.4 | 10.3 | 1.2 | 0.1 |
| 12 | 3.48 | 91.5 | 6.7 | 1.7 | 0.2 |
| 13 | 3.75 | 94.0 | 4.0 | 1.8 | 0.2 |
| Ref. | 3.57 | 76.2 | 22.5 | 1.1 | 0.2 |

* 4H-DBT: tetrahydrodibenzothiophene.

** 6H-DBT: hexahydrodibenzothiophene.

**Table 5** Catalytic activities in HDS reactions of 4,6-DMDBT

| | HDS Rate | Product Distribution | | | |
|---|---|---|---|---|---|
| R | (x $10^6$ mol.gcat$^{-1}$.s$^{-1}$) | 3,3'-DMCHB* (%) | 3,3'-DMBP** (%) | 4H-DMDBT** (%) | Cracking Products (%) |
| 3 | 0.133 | 85.8 | 7.9 | 6.3 | 0 |
| 4 | 0.206 | 77.8 | 8.9 | 11 | 2.3 |
| 5 | 0.192 | 85.8 | 11.6 | 2.6 | 0 |
| 6 | 0.229 | 83.8 | 13.5 | 2.7 | 0 |
| 7 | 0.460 | 79.5 | 7.8 | 1.4 | 11.3 |
| 8 | 0.466 | 82.3 | 9.4 | 0.8 | 7.5 |
| 9 | 0.775 | 85.8 | 6.9 | 0.5 | 6.8 |
| 10 | 0.628 | 86.3 | 5.8 | 0.7 | 7.2 |
| 11 | 0.256 | 84.4 | 13.9 | 1.7 | 0 |
| 12 | 0.335 | 85.5 | 13.3 | 1.2 | 0 |
| 13 | 0.226 | 85.4 | 6.6 | 8 | 0 |
| Ref. | 0.831 | 88.4 | 11.3 | 0.3 | 0 |

* 3,3'-Dimethylcyclohexylbenzene, including trace amounts of 3,3'-dimethylbicyclohexyl (3,3'-DMBCH).
** 3,3'-Dimethylbiphenyl.
*** Tetrahydro-dimethyldibenzothiophene, including trace amounts of hexahydro-dimethyldibenzothiophene (6H-DMDBT) (less than an absolute value of ~ 0.2 %).